SESSION 6. COMPUTER GRAPHICS

Session Chairman

W. J. Batdorf

Lockheed Georgia Co.
Marietta, Georgia

DISPLAYS OF KINEMATIC AND ELASTIC SYSTEMS

by

*Henry N. Christiansen**
Brigham Young University, Provo, Utah and
University of Utah, Salt Lake City, Utah

This paper reports on a continuing exploration of computer graphics techniques as they apply to the analysis of kinematic and elastic systems. The report deals with two aspects of the work; the creation of a simulator for kinematic and elastic systems, and the utilization of computer graphics software and hardware to produce continuous tone images. The simulator is a computer program which utilizes a linear finite element stiffness model to achieve exact solutions for large displacement kinematic problems of foldable plates and trusses, as well as approximate solutions for large displacement, small strain, elasticity problems. Various techniques associated with the production of continuous tone images have been utilized to aid in the display of stress, strain, and/or displacement results producible with the simulator and other finite element programs.

**Professor of Civil Engineering Science, BYU, and Research Associate Computer Science, Univ. of Utah.*

SECTION 1

INTRODUCTION

The original purpose of this study was to develop a computer program which would simulate the kinematic and elastic behavior of foldable plate and truss structures. The more recent purpose has been to explore possibilities for displays of the output of the simulator and other finite element programs.

The requirement for the simulator was generated by Resch[1] who created what he terms "kinematic folded plate systems." The commom property of these systems is that, by allowing only folding along the edges of a continuous line pattern, a flat sheet may be transformed into a variety of three dimensional shapes. Figure 1 illustrates a paper model of one system which is a repetition of only two non-identical plate elements. Figure 2 shows another pattern which requires four non-identical elements. These systems give promise of the mass production of non-identical structures of unusual beauty and structural efficiency.

Resch's initial investigation involved the manual folding of sheets of paper upon which the pattern had been scribed. The model could then be moved by hand to produce a variety of shell forms. When a desirable shape was obtained, the system could be stabilized by providing sufficient supports or the addition of truss and/or plate elements. These constraining systems change the character of the motion of the model from kinematics to elastic deformation.

This approach, while yielding pleasing visual effects, had several drawbacks. First, the process required repetition (the model shown in Figure 1 took 30 hours to fold) to investigate any parameter change in the "wrinkle" definition. Second the dimensions of elements added to stabilize the shell are unique to the shape chosen. Thus, each element had to be individually measured and created to fit the kinematic pattern. Inaccuracy in this process prevented duplication of a particular configuration. Finally, while the investigators were impressed with the apparent stiffness of the stabilized shells, the model was not useful in an analysis of stress and strain.

The functions of kinematic and elastic analysis were accomplished as a result of a finite element stiffness approach to the linear elasticity problem. Developments which allow this approach include the modeling of the folds as elastic hinges and the generation of applied force systems which tend to restore the original dimensions of the elements.

Upon completion of the simulator, effort was directed toward the utilization of the ability to produce continuous tone pictures to display the stress, strain and displacement results of the finite element solutions producible with the simulator and other programs. Three methods of data presentation were devised and developed. In the most primitive mode, the object is displayed under load and variation of the light intensity of the surface of the object is utilized to indicate the level of stress or strain.

Figure 1. Folded Plate System with Two Non-Identical Elements

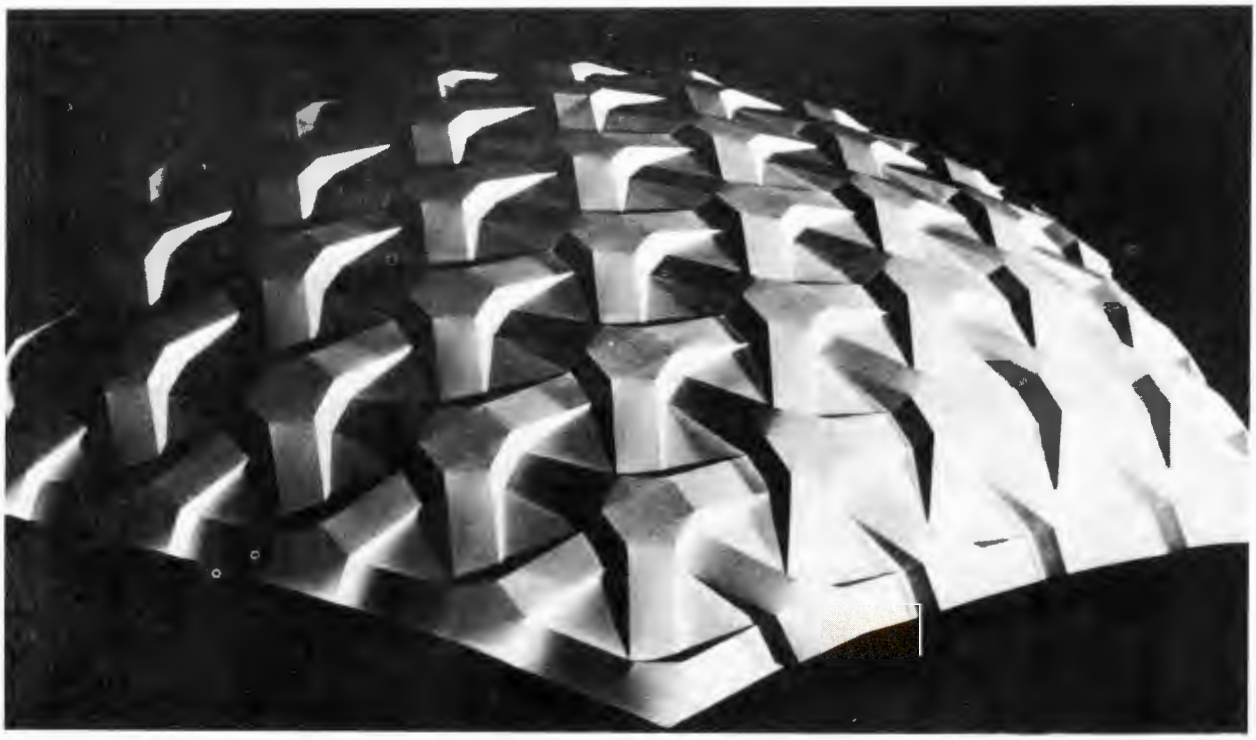

Figure 2. Folded Plate System with Four Non-Identical Elements

A variation on this scheme results from making the light intensity proportional to the square of a harmonic function of the selected stress or strain component. In this way fringe effects develop which have a character much like that produced using photo-elastic techniques. In another scheme the object is warped such that the out of plane coordinate is proportional to the stress or strain function. The resulting three dimensional shape is displayed in a conventional manner. The results of these efforts are discussed and displayed in following sections.

SECTION II

STRUCTURAL ANALYSIS OF KINEMATIC FOLDED PLATE SYSTEMS

Two major functions are performed in the structural analysis of folded plate structures. The first function is the large displacement kinematic analysis associated with positioning the structure in the desired shape. The second function is the small displacement elastic analysis of the properly positioned and stabilized structure. While both functions are accomplished as a result of a finite element stiffness method approach to the small displacement elasticity problem, the large displacement kinematics analysis requires a repeated application of the linear theory.

Kinemavic analysis is achieved by:

1) modeling the plates as constant strain, plane stress elements and the folds as flexible springs,

2) performing an elastic analysis,

3) adding the computed displacements to the nodal coordinates,

4) computing nodal force systems which tend to restore the plate (or truss) element dimensions, and

5) repeating steps 1 thru 4 until convergence is achieved.

When the fold element is not restored (i.e. no attempt is made to reestablish the original angles between the elements) convergence is either to a kinematically possible configuration or to the large displacement, small strain, elasticity solution. The elasticity solution results when the prescribed displacements are not possible through rigid body motions of the individual structural elements. In either case, the fold elements will be unstressed during the final iteration. If the fold elements are restored, convergence is to an elasticity solution.

After each iteration, the displacement constraints may be modified. Thus, the solution achieved is a function of the order in which the constraints are applied and removed. When the desired kinematic arrangement is achieved, the structure is stabilized with additional elements and/or displacement constraints. Additional iterations may then be performed, for specified loading systems, to obtain elastic displacements and stresses.

Much of this procedure is inherent in any finite element analysis and has been documented many times. To prevent an additional redundancy only those parts of the procedure which are thought to be at least relatively unknown are described in this paper. Two developments are judged to be in this category. The first is the definition of a stiffness matrix for a fold element and the second is the procedure by which corrective forces are generated.

STIFFNESS MATRIX FOR A FOLD ELEMENT

In this formulation, the fold between two triangular elements (see Figure 3) is assumed to have a stiffness (i.e. resistance to folding) which increases linearly with the fold length.

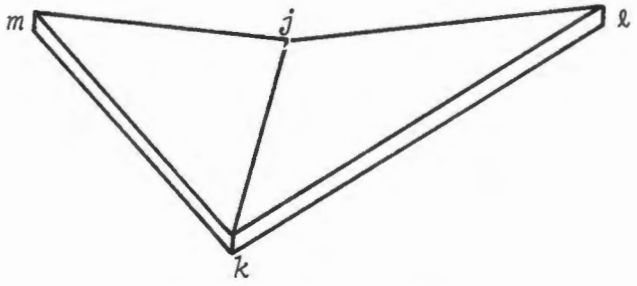

Figure 3 Fold Element jklm

The strain energy associated with this stiffness is equal to the work done by a system of force couples M in decreasing the dihedral angle between the two plate elements by the small angle θ and is thus written as

$$U = \frac{1}{2} M \theta \qquad (1)$$

The assumed stiffness suggests a generalized force-displacement relationship of the form

$$M = KL\theta \qquad (2)$$

where K and L are the stiffness per unit length and length of the fold. With this substitution, the strain energy is

$$U = \frac{1}{2} KL \begin{Bmatrix} \theta_\ell \\ \theta_m \end{Bmatrix}^T \begin{bmatrix} I \end{bmatrix} \begin{Bmatrix} \theta_\ell \\ \theta_m \end{Bmatrix} \qquad (3)$$

where θ_ℓ and θ_m are the rotations about the axis jk of elements jkℓ and jkm, and

$$\left[I \right] = \begin{bmatrix} 1 & -1 \\ -1 & 1 \end{bmatrix} \tag{4}$$

The next step is to express the rotations in terms of the nodal displacement components. Starting with element jkℓ and introducing a local coordinate system (X_i) as shown in Figure 4,

$$\left\{ \theta_\ell \right\} = \left[\bar{X}_\ell \right] \left\{ U'_\ell \right\} \tag{5}$$

where

$$\left\{ U'_\ell \right\} = \begin{Bmatrix} U'_{3j} \\ U'_{3k} \\ U'_{3\ell} \end{Bmatrix}, \quad \left[\bar{X}_\ell \right] = \frac{1}{LX'_{2\ell}} \begin{bmatrix} (X'_{1\ell}-L) & (X'_{1\ell}) & (L) \end{bmatrix},$$

and U'_{3i} is the displacement in the X'_3 direction at node i.

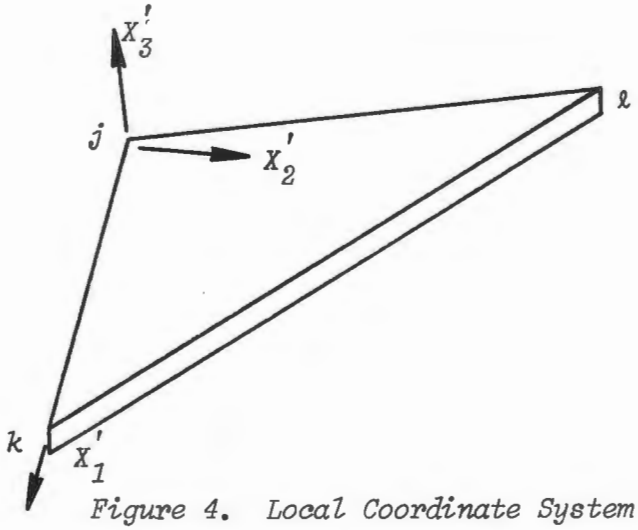

Figure 4. Local Coordinate System X'_i

In like manner (see Figure 5) for element jkm

$$\left\{ \theta_m \right\} = \left[\bar{X}_m \right] \left\{ U''_m \right\}, \tag{6}$$

where

$$\left\{U''_m\right\} = \begin{Bmatrix} U''_{3j} \\ U''_{3k} \\ U''_{3m} \end{Bmatrix}, \quad \left[\bar{X}_m\right] = \frac{1}{LX''_{2m}} \left[(X''_{1m} - L) \;\; (-X''_{1m}) \;\; (L)\right]$$

and U''_{3i} *is the displacement in the* X''_3 *direction at node i.*

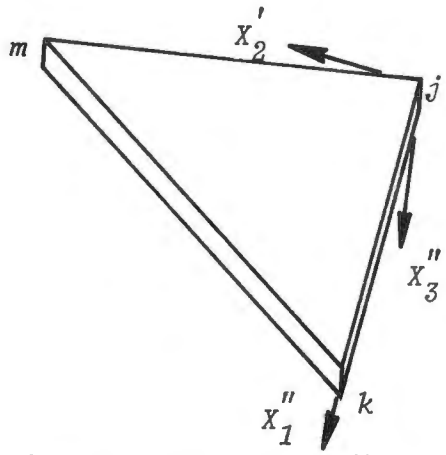

Figure 5. Local Coordinate System X''_i

Combining the rotation-node displacement relationships

$$\begin{Bmatrix} \theta_\ell \\ \theta_m \end{Bmatrix} = \begin{bmatrix} \bar{X}_\ell & \\ & \bar{X}_m \end{bmatrix} \begin{Bmatrix} U'_\ell \\ U''_m \end{Bmatrix} \tag{7}$$

Transformation to the global coordinate system displacement components is facilitated by

$$\begin{Bmatrix} U'_\ell \\ U''_m \end{Bmatrix} = \left[D\right] \left\{U\right\} \tag{8}$$

where

$$\left\{U\right\}^T = \left\lfloor U_{1j} \; U_{2j} \; U_{3j} \; U_{1k} \; U_{2k} \; U_{3k} \; U_{1\ell} \; U_{2\ell} \; U_{3\ell} \; U_{1m} \; U_{2m} \; U_{3m} \right\rfloor,$$

$$[D]=\begin{bmatrix} d'_{31} & d'_{32} & d'_{33} & & & & & & \\ & & & d'_{31} & d'_{32} & d'_{33} & & & \\ d''_{31} & d''_{32} & d''_{33} & & & & d'_{31} & d'_{32} & d'_{33} \\ & & & d''_{31} & d''_{32} & d''_{33} & & & \\ & & & & & & & & d''_{31} \; d''_{32} \; d''_{33} \end{bmatrix}$$

U_{in} *is the displacement in the* X_i *(global coordinate) direction at node* n, *and* d'_{3i} *and* d''_{3i} *are cosines of the angles between the* X_i *axis and the* X'_3 *and* X''_3 *axes respectively.*

With this substitution, the rotation-node displacement relationship is

$$\begin{Bmatrix} \theta_\ell \\ \theta_m \end{Bmatrix} = \begin{bmatrix} \bar{X}_\ell & \\ & \bar{X}_m \end{bmatrix} [D] \{U\}, \tag{9}$$

and the strain energy expression becomes

$$U = \frac{KL}{2} \{U\}^T [D]^T \begin{bmatrix} \bar{X}_\ell & \\ & \bar{X}_m \end{bmatrix} [I] \begin{bmatrix} \bar{X}_\ell & \\ & \bar{X}_m \end{bmatrix} [D] \{U\} \tag{10}$$

The stiffness matrix, by application of the principle of virtual displacements, is

$$[K] = KL [D]^T \begin{bmatrix} \bar{X}_\ell & \\ & \bar{X}_m \end{bmatrix}^T [I] \begin{bmatrix} \bar{X}_\ell & \\ & \bar{X}_m \end{bmatrix} [D] \tag{11}$$

CORRECTION FORCES SYSTEMS

The plane stress triangular element requires correction forces which will restore the original length of each side of the triangle. Since the columns of the element stiffness matrix are the sets of force systems required to produce individual unit nodal displacements components, by

expressing the change in length of each side of the triangle in terms of an equivalent set of nodal displacement components, a set of corrective forces may be obtained. This corrective nodal force component vector is given by the negative of the product of the element stiffness matrix and the equivalent set of nodal displacement components.

To achieve the equivalent set of nodal displacement components, displacement modes which each represent the elongation of a single side of the triangle are introduced as illustrated in Figure 6 a, b, and c.

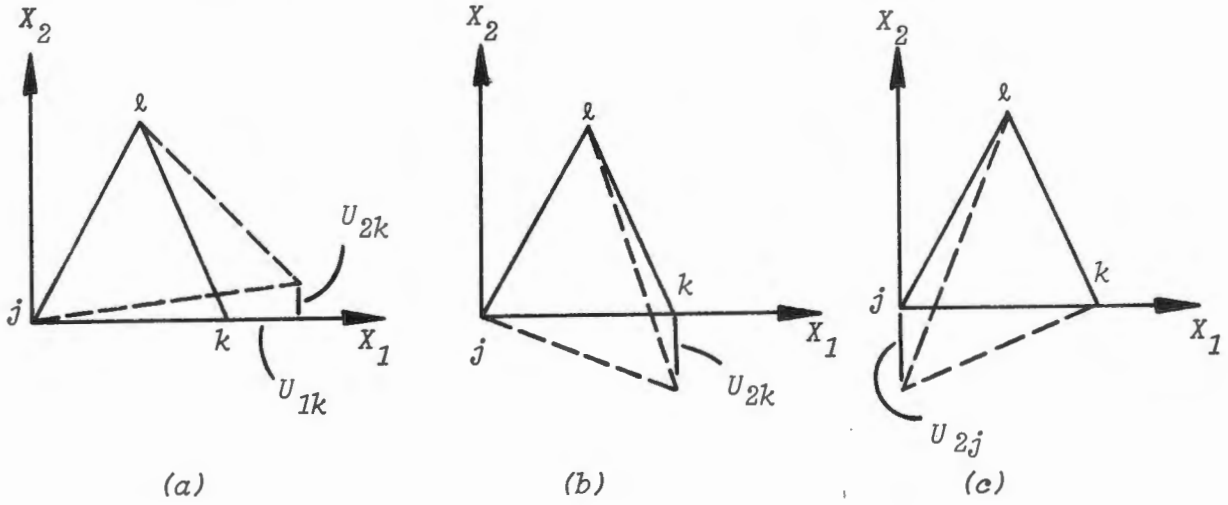

Figure 6. Side Elongation Modes for Triangular Elements

In the coordinate system shown, Figure 6a depicts a mode for which sides jℓ and kℓ have been preserved in length and side jk has been stretched. Figure 6b illustrates a set of nodal displacement components for which sides jk and jℓ are preserved in length and side kℓ is stretched. Figure 7c shows sides jk and kℓ unstretched and side jℓ stretched. Letting δ_{jk}, $\delta_{j\ell}$, and $\delta_{k\ell}$ represent the change in length of sides jk, jℓ, and kℓ respectively as calculated from the current and original nodal coordinates, the relationship between the nodal displacement components and the side elongations is

$$\begin{Bmatrix} U_{1j} \\ U_{2j} \\ U_{1k} \\ U_{2k} \\ U_{1\ell} \\ U_{2\ell} \end{Bmatrix} = \begin{bmatrix} & & -L_{j\ell}/X_{2\ell} \\ 1.0 & & \\ (X_{1k} - X_{1\ell})/X_{2\ell} & & -L_{k\ell}/X_{2\ell} \end{bmatrix} \begin{Bmatrix} \delta_{jk} \\ \delta_{j\ell} \\ \delta_{k\ell} \end{Bmatrix} \qquad (12)$$

Transformation of this system of nodal displacement components to the global coordinate system is achieved by the use of the proper direction cosine matrix. The nodal force system is then computed by a premultiplication of the displacement components by the element stiffness matrix.

If the fold element is to be restored, the change in the angle of the fold is computed and a corresponding set of nodal displacements is introduced. For the coordinate systems shown in Figures 4 and 5, this set is simply $U'_{3\ell} = -\Delta\Theta\, X'_{2\ell}$. A transformation to the global coordinate system and premultiplication by the fold element stiffness matrix generates a set of force couples which (if structure were otherwise unconstrained) are the small displacement approximation of the forces required to produce the observed fold opening. The correction force system is the negative of this vector.

Judgment of convergence is made by the user from a print-out of the largest absolute relative kinematic errors in the truss, triangle, and fold elements. For kinematic analysis the error associated with the fold element is ignored. Experience suggests that for rather large imposed displacements the first or second iteration solution is satisfactory for viewing purposes. Depending upon the constraints on the structure, it is normal for the kinematic error to reduce an order of magnitude for each successive iteration until limited by machine accuracy.

SECTION III

COMPUTER GENERATED DISPLAYS

Following the adage that "a picture is worth a thousand words," the past decade has seen the emergence of the field of computer graphics. The early work centered around the problems associated with the reduction of three dimensional data onto a two dimensional surface. The problem of perspective was treated by Smith[3] and Johnson[4], and a significant improvement was made by Roberts[5] with the elimination of hidden lines performed at a reasonable cost. Another important advance came as a result of the introduction of shaded pictures at the University of Utah (Romney[6], Warnock[7], and Watkins[8]), GE[9] and MAGI[10].

COMPUTER GENERATION OF CONTINUOUS TONE PICTURES

Computer generation of continuous tone images refers to the rendering of shaded objects by means of a raster driven cathode ray tube. The discussion is limited to a point source of illumination located at the eye-point so as to avoid the complication of shadows. The images produced are recorded by a camera mounted in front and pointed at the screen. As the images are being computed and displayed one line at a time (the pictures in this paper have 1024 lines), the camera, with the lens open, performs an integration function.

Hidden surfaces are removed as a result of comparisons of elements in the scene in order to determine which is in front of which. A simplification is obtained by applying a perspective transformation such that the observer is located at infinity in the direction of the Z axis, reducing the problem to a comparison of Z coordinates.

Some systems have been devised (MAGI[10], Comba[11], Weiss[12], and Mahl[13]) which have the capability to remove hidden parts for curved surfaces by restricting the class of possible surfaces or accepting long execution times. Recently at the University of Utah, Gouraud[14] perfected a method which uses a small polygon approximation of the surface to solve the hidden surface problem and then computes the shading on each polygon according to a linear function such that visual discontinuities between adjacent polygons disappear. The method (used in pictures shown in this paper) is both general and efficient.

SECTION IV

DISPLAYS OF KINEMATIC SYSTEMS

Figure 7 is a photograph of a computer generated continuous tone picture of a typical kinematic folded plate system. This hexagonal arrangement of approximately 600 triangular elements is shown in what has been termed "the flat configuration." That is, in this very regular geometry, the equilateral triangle elements all lie in a common plane.

Starting with the flat configuration, systems of constraints are applied to create various shapes. Figures 8, 9, and 10 indicate the dome like configurations achieved by holding nodes on the outer edge of the pattern and raising the center node. Characteristically, such shapes have quite uniform "star patterns" in the shallow dome configuration and non-uniform openings in the deep shell configuration.

Figure 10 shows an extension of the system which is close to the kinematic limit. That is, if the center node is raised much higher, pop-thru (a local buckling) of the star pattern will occur and/or convergence will be to an elasticity solution. Pop-thru (which is monitored by the simulator) is difficult to control and once begun often produces oscillations in the computational process.

Figures 11 and 12 show a warped effect which has been achieved by holding the center node and alternately raising and lowering the six corner nodes of the hexagonal system.

In both modes of behavior, there are six axes of geometrical symmetry which considerably reduces the computational problem for the simulator. However, as a perspective view of the structure is being created for an arbitrary point of observation, structural symmetry cannot be taken advantage of by the hidden surface routine.

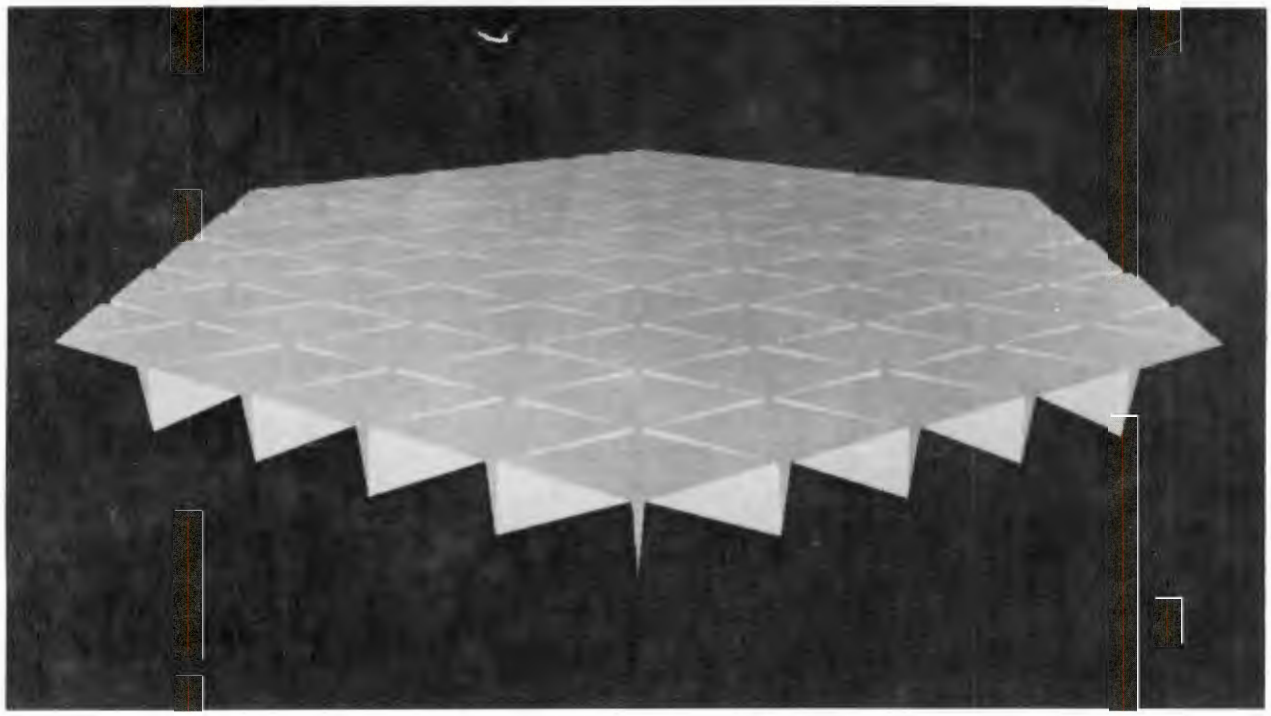

Figure 7. Flat Configuration

Figure 8. Shallow Dome

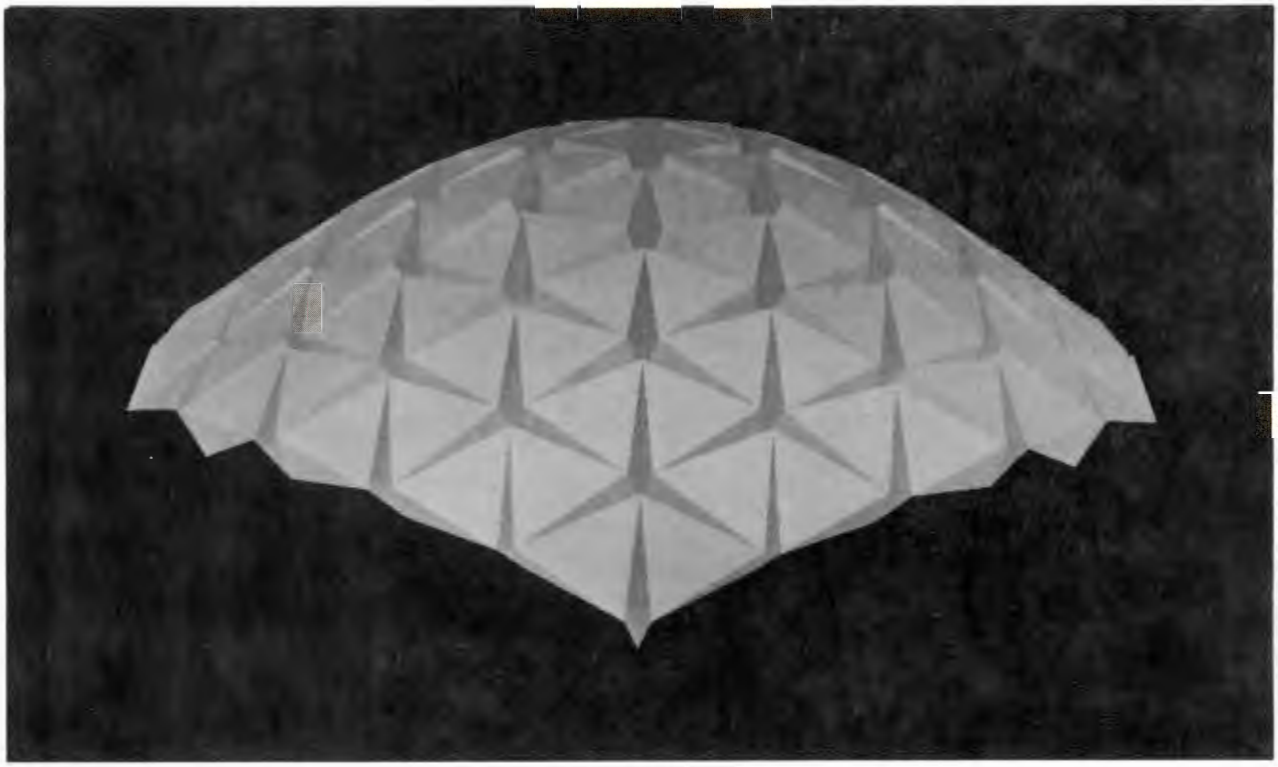

Figure 9. Intermediate Dome

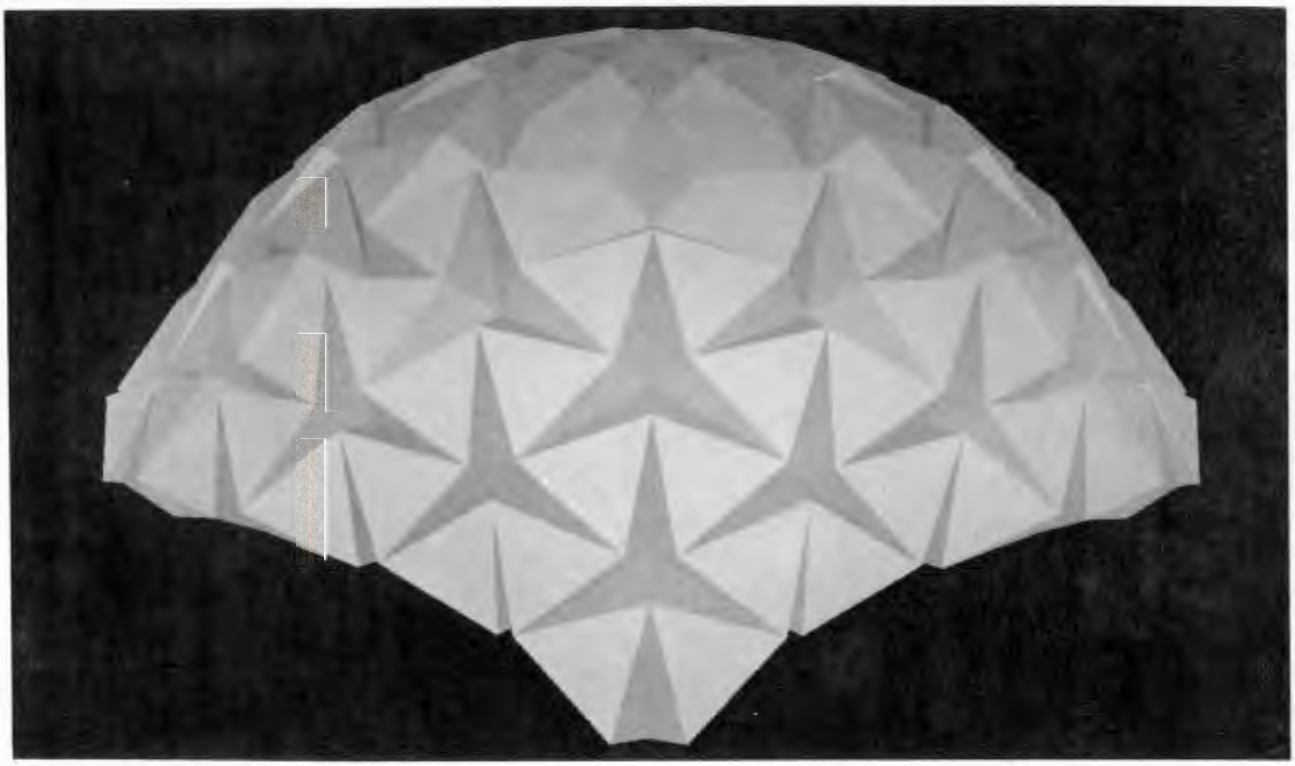

Figure 10. Deep Dome

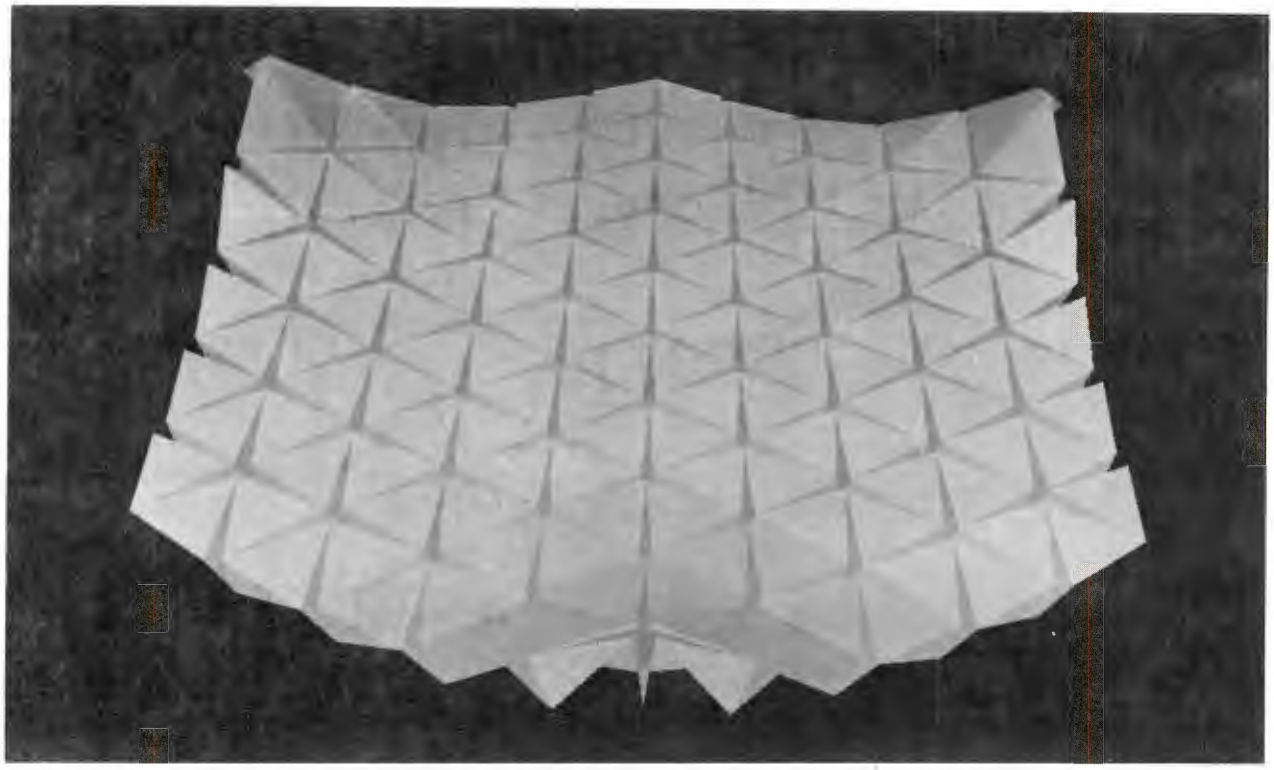

Figure 11. Slightly Warped System

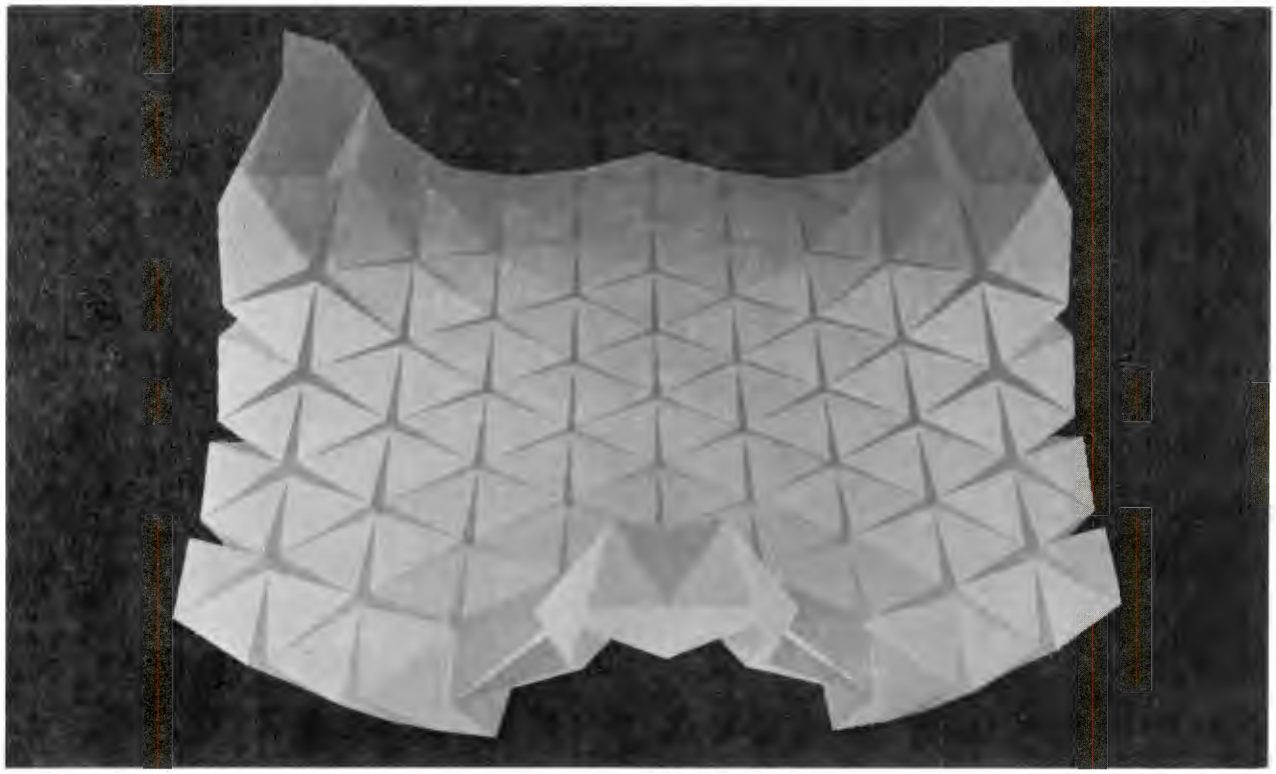

Figure 12. Highly Warped System

SECTION V

DISPLAYS OF ELASTIC SYSTEMS

INTRODUCTION

One compelling attraction of the photo-elastic technique is that it allows the analyst the opportunity to "see the stresses." With the thought that this benefit might be made available to finite element users, a study was launched into possible schemes for the presentation of stress, strain and/or displacement data available in a discrete digital format.

It was apparent that displacement data could readily be displayed in the form of a continuous tone picture of a highly distorted structure. The problem, then, centered upon ways to superimpose stress or strain information on the distorted geometry. Three methods have, so far, emerged from this effort. The first two involve the variation of the light intensity of the surface to indicate the stress or strain level. The third involves geometry modifications to accomplish the same purpose. Each method has, so far, only been applied to plane stress problems.

In each method, the data may be displayed in a "flat" or "smooth" manner. The "flat" presentation preserves the identification of the individual elements by "painting" the entire element the same average light intensity. "Smooth" shading utilizes the recently developed curved surface capability to create the illusion of continuous stress or strain variations. This is accomplished by employing linear interpolation to the light intensities computed for each corner node. In each of the pictures presented in this section, both formats are shown.

To facilitate these two formats, the elastic analysis capability of the simulator was modified in two ways. First, a quadrilateral element (composed of four constant strain triangular elements) was introduced. This element is more convenient with respect to automatic grid generation and provides relief from the grid bias problem. Second, the procedure utilized to calculate element stress and strain was changed. In order to achieve node values instead of element values, the standard procedure of premultiplying the displacement vector by stress matrices, was replaced by a least square fit routine. This procedure allows the prediction of strain components as a result of "fitting" the node displacement components with an incomplete cubic polynomial in the in-plane coordinates. The function, based upon a local coordinate system, is

$$u_i = a_{i1} + a_{i2}x + a_{i3}y + a_{i4}x^2 + a_{i5}xy + a_{i6}y^2 + a_{i7}x^2y + a_{i8}xy^2$$

The "fit" is applied to a local set of nine nodes.

The initial scheme involved the shading of the elements according to the magnitude of the stress or strain component selected for presentation. Elements with a high value appear bright (i.e. highly reflective) and those with a low value appear relatively dark.

Experimentation suggests this to be a good procedure whenever high gradients are involved. For this reason, the method is useful in the display of beam problems. For these simulations, the most effective function for display is maximum shear stress (or strain). This function allows the combined display of the bending moments and shear diagrams. At the neutral-axis, the maximum shear stress is equal to the absolute value of the shear stress on the cross section and thus (at least for uniform beams) proportional to the shear diagram. At the top and bottom fibers, where shear stress on the cross section and the lateral normal stress components are both zero, the maximum shear stress is equal to one-half the absolute value of the axial stress component and, thus, monitors the bending moment diagram.

Figure 13 illustrates the "flat" and "smooth" shading of a uniform beam with "built-in" end conditions. The model, containing 504 quadrilateral elements, was assigned a modulus of elasticity of 28 million psi and Poisson's ratio of 0.25. The desired level of displacement was achieved by the specification of the displacement magnitude of the quarter span location. By scanning along the upper or lower edge of the beam, four changes in sign of the bending moment diagram can be observed. Repeating the scan along the neutral axis shows uniform shear with abrupt changes in sign at the three load locations (indicated by computer generated arrows). The "smooth" shaded picture, especially, suggests a local drop in the maximum shear stress under the one-quarter span loads. This is because the axial and lateral stress components are both approximately the same negative value, which results in a small value for the maximum shear stress. At mid-span the lateral and axial stress components are unequal and a local maximum is observed.

Figure 14 shows a beam with linearly tapered segments. This model also contains 504 elements with a modulus of elasticity of 10 million psi and Poisson's ratio of 0.15. Like the uniform beam this problem was posed in the form of specified nodal displacements and symmetry was utilized to reduce the computational effort. Note the very local compression at the tips of the beam and the interesting stress distribution above the supports.

Since this shape is not as familiar as the uniform section beam, the observer may lose track of the undistorted shape if large displacements are displayed. For example, many observers of this picture are uncertain of the linear taper for the unloaded geometry. On the other hand, the display of small displacements leaves the distortion pattern in doubt. The conflict is not easily resolved.

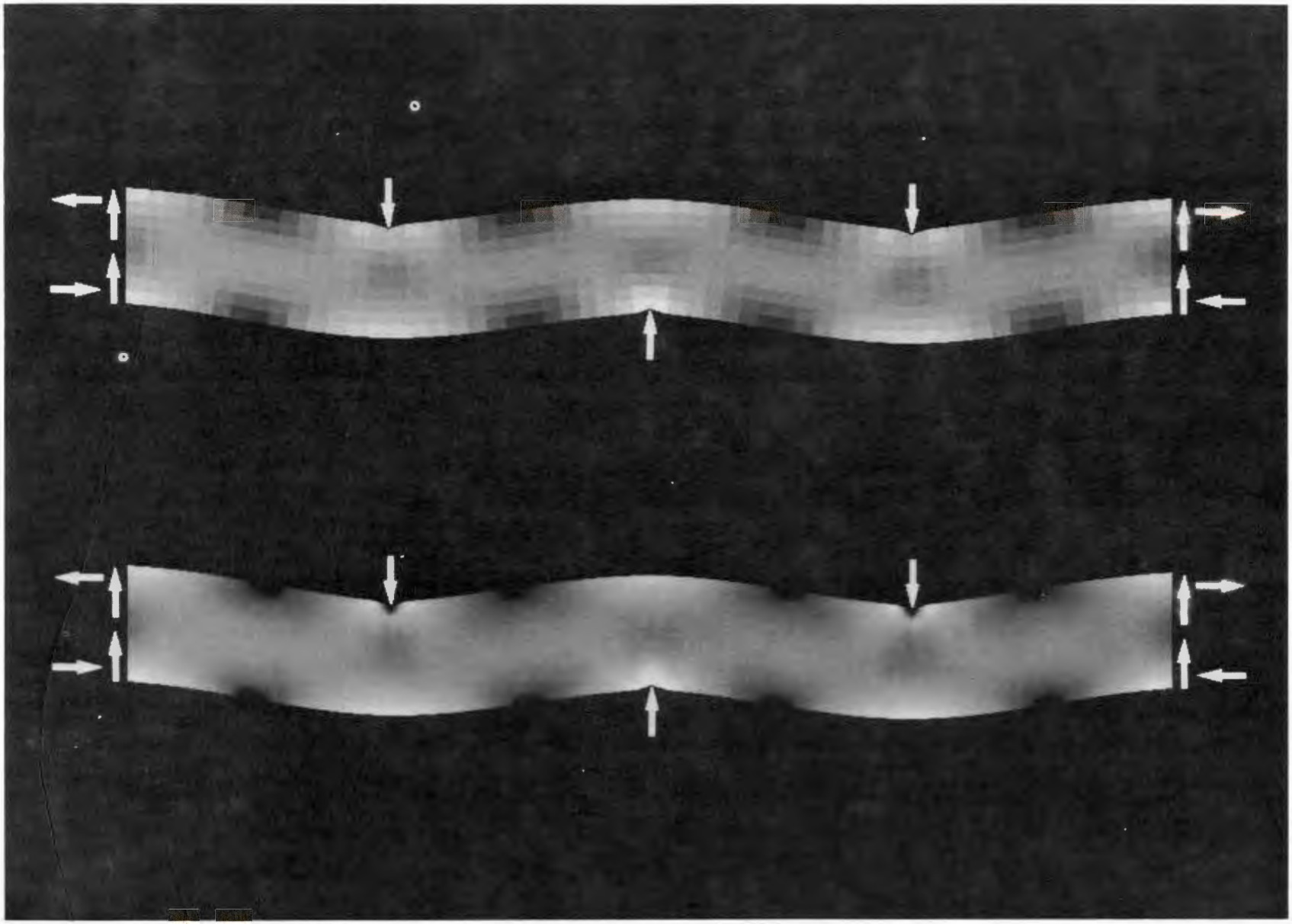

Figure 13. Uniform Beam

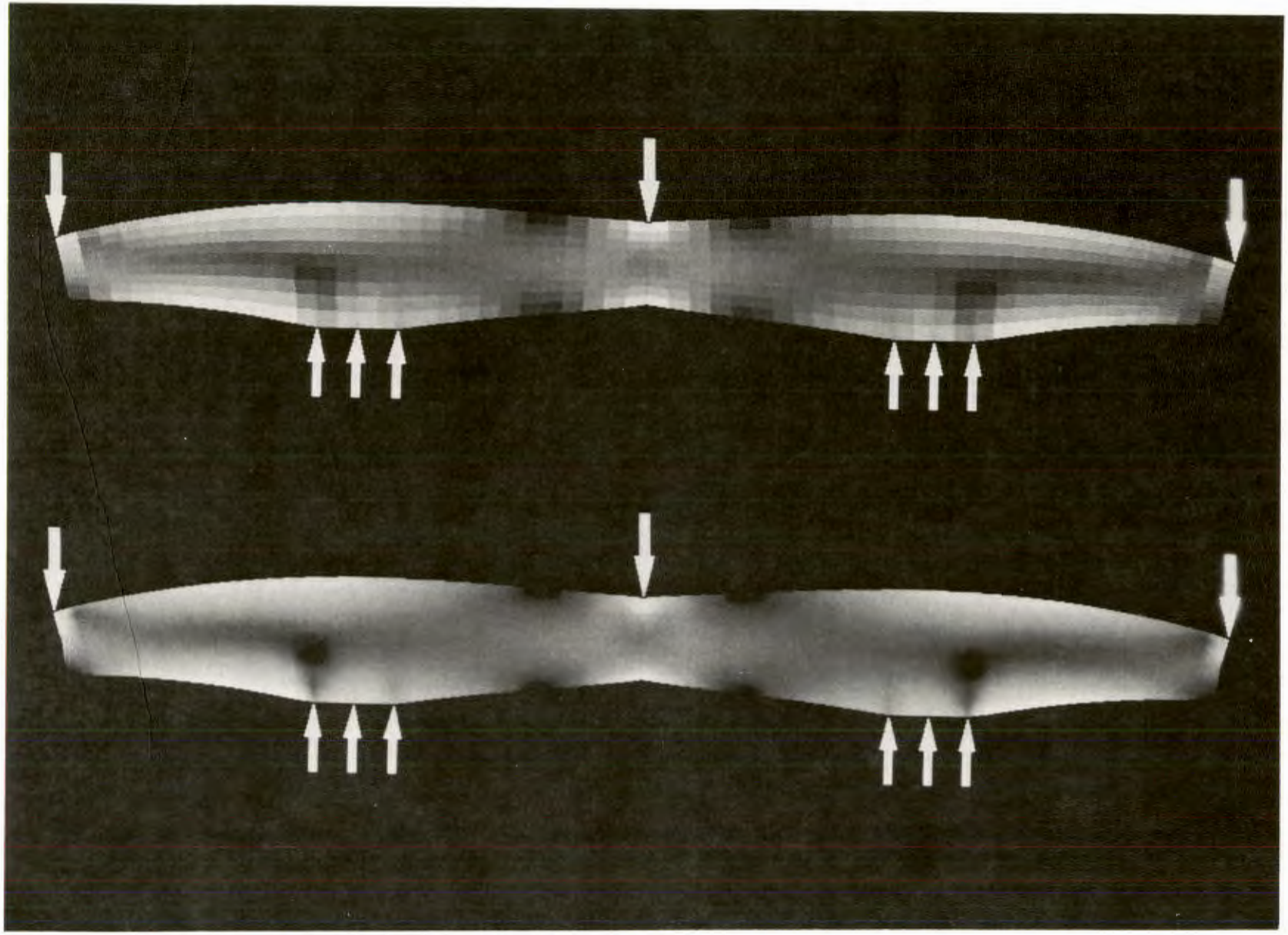

Figure 14. Tapered Beam

FRINGE PATTERNS

A modest change in the "black to white" scheme results in the display of fringe patterns. The effect is not unlike experimental stress optic patterns but has the advantage that the user may display the stress or strain component of his choice. The modification is to display a new function, ϕ, instead of the stress, σ, where,

$$\phi = \cos^2(\alpha\sigma+\beta)$$

The constants α and β are chosen so as to select a particular number of fringes and to shift the pattern.

Figures 15 and 16 illustrate this technique applied to the analysis of thin plate configurations. In both examples the modulus of elasticity is 1 million psi, Poisson's ratio is 0.45, and there are two axes of geometrical and loading symmetry. The function displayed is the maximum principal stress.

Figure 15 is a perspective representation of a rectangular (45 by 30 inch) plate with a circular hole (diameter 15 inches). The model contains 800 quadrilateral elements. The axial load varies from 66,700 psi at the center to zero at the outer edges. A complete shading cycle (white to black to white) represents a stress change of 50,000 psi.

Figure 16 illustrates a perspective view of a strip containing a circular ring section. The overall length is 8.4 inches, the width at the end is 2.4 inches and the diameter of the hole is 3.5 inches. The model contains 840 elements. The loading is a uniform axial stress of 20,000 psi. In this picture a complete shading cycle represents a stress change of 75,000 psi.

The main drawback in this format is the lack of identification of the stress level associated with any particular fringe. That is, if one scans from white to black, he may not know if the stress level has increased or decreased. Further, if he continues the scan into a new white zone, has he changed fringes? Color variation in parallel with light variation is currently being investigated as a possible solution to this problem.

A similar effect has recently been achieved by Sanford[15] who produced computer generated holographic interference patterns for known theoretical stress solutions. His patterns are shown in the undistorted geometry. An interesting contrast with Sanford's work is that, with closed form solutions, the analyst may ask for more fringes and (until the fringe width approaches the resolution of the equipment) he gets them. However, with finite element results, to ask for a large number of fringes usually results in a random pattern that looks much like a very poor quality Navajo rug.

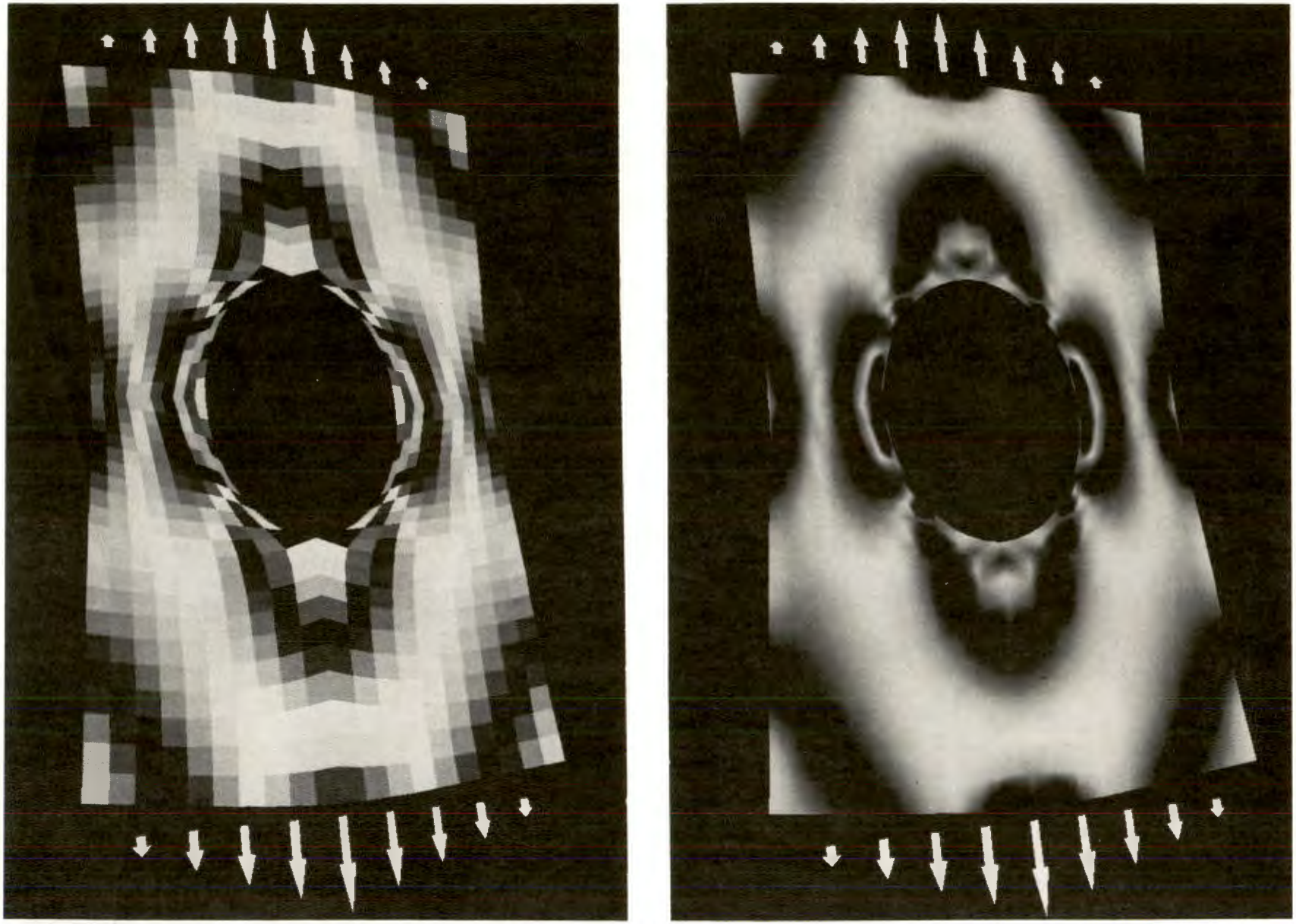

Figure 15. Plate with Circular Hole

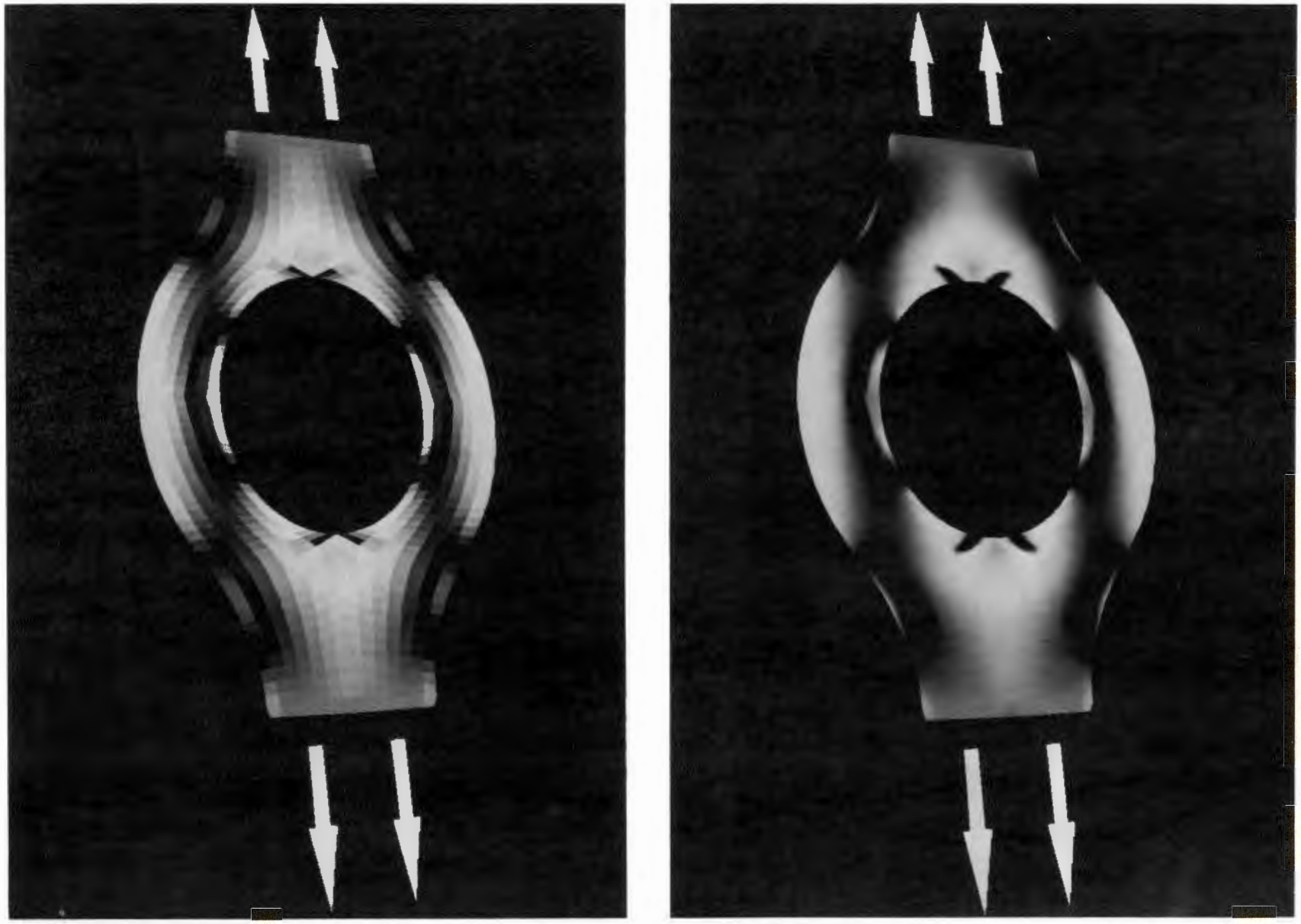

Figure 16. Strip with Circular Ring Section

WARPED SURFACES

The previously described display formats utilized variation in the light intensity of the surface to describe a chosen stress or strain function. An alternate procedure is to introduce geometry modifications in the form of computed out of plane coordinates which are proportional to the stress or strain function. This seems natural as functions of two variables are often displayed as a surface whose height above the reference plane is proportional to the function. Light variation is also utilized, but now to indicate the angle between the normal to the surface and the direction to the illumination source (the eye of the observer). For "flat" shading, the element normal is chosen as the average of the four normals computed on the basis of vector products of the adjacent sides. This average normal is also the normal obtained by the vector product of the diagonals of the quadrilateral. For the "smooth" shading version, the least square fit routine is again utilized to obtain normals at each node.

Figures 17 and 18 illustrate this display format for the problems previously discussed and displayed in a fringe effect format in figures 15 and 16.

In viewing this display form, the observer is acutely aware of the apparent stress concentrations (perhaps for the first time). While stress concentrations and sharp gradients do occur in these regions, the shapes displayed are dependent upon the local element definition and behavior of the least square fit procedure as utilized to generate strain values.

Comparing the "flat" and "smooth" shading versions, in the vicinity of the stress concentrations, suggests that very good definitions of curved surfaces may be developed from rather crude models. This is generally true. However, several drawbacks are also apparent. If this were the only display format available each picture would have to be accompanied by an undistorted picture to describe the geometry. Further it is difficult to find a satisfactory viewing angle and magnitude of distortion. The problem is somewhat compounded by the errors made by the hidden surface routine in the form of small holes in the surface. These errors apparently arise from difficulties the routine has in treating highly warped quadrilateral elements in a complex hidden surface environment.

It is expected that this form of display will come into its own when movies are made showing the transition from the undistorted to distorted geometry and allowing the observer to see the surface from many angles.

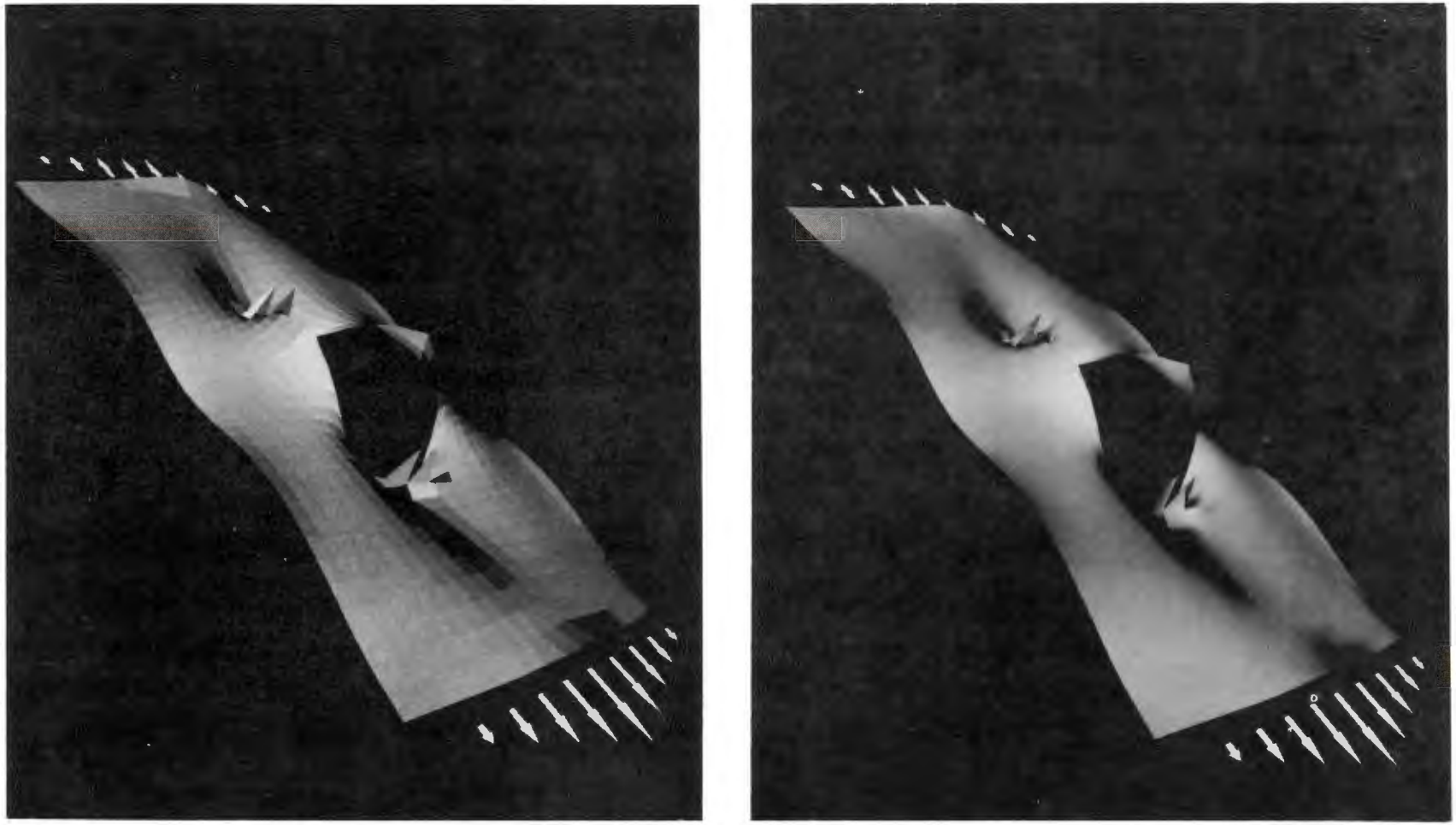

Figure 17. Flat Plate with Circular Hole

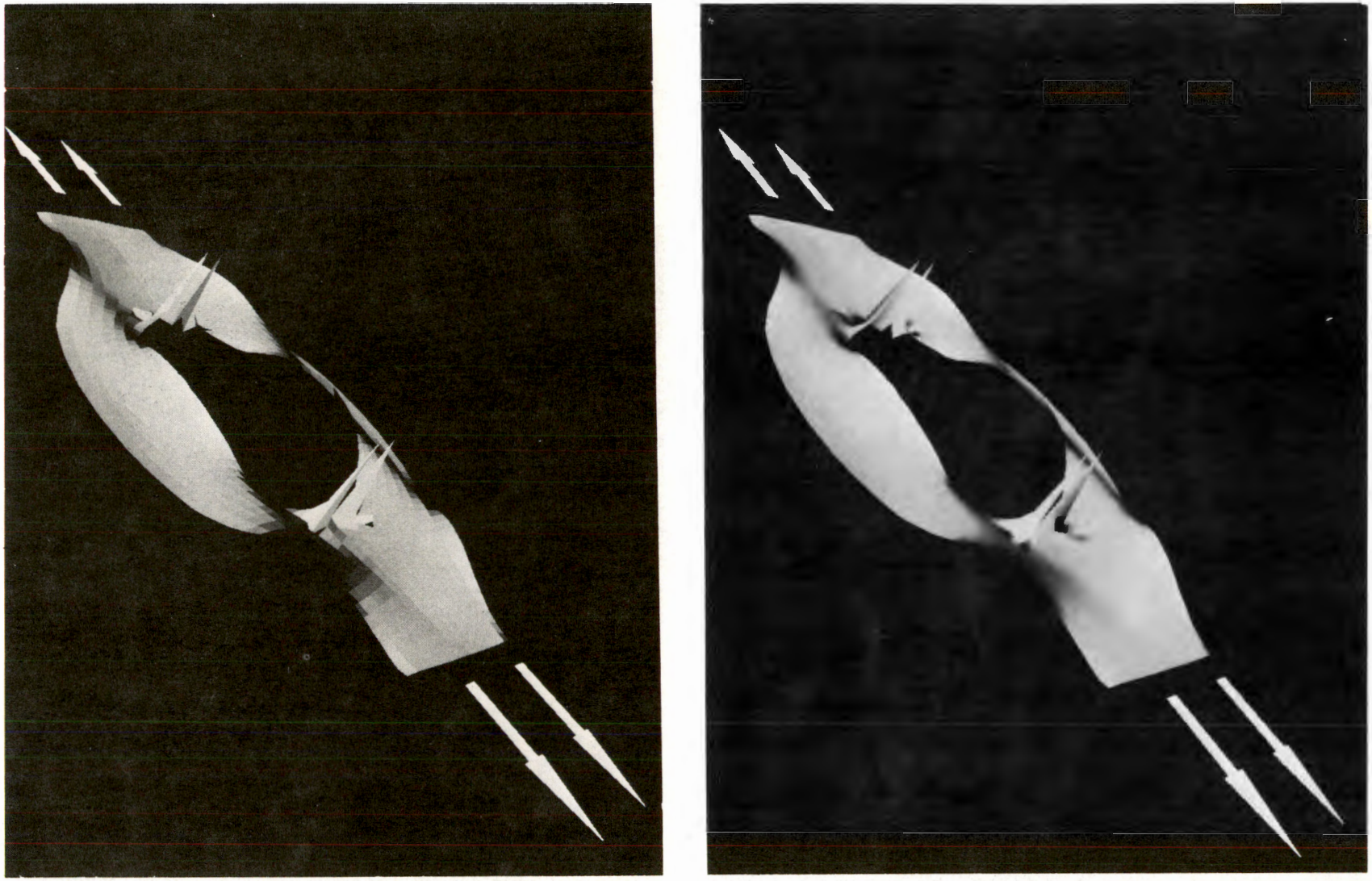

Figure 18. Strip with Circular Ring Section

SECTION VI

CONCLUDING COMMENTS

Usage to date suggests that a repeated linear analysis which employs the concept of corrective forces is an effective way to solve kinematic problems. Indeed, rapid convergence to an exact result has been the usual experience. Nevertheless, a greater potential is envisioned for the display techniques. Even here, the most likely occurrence is the development of superior methods of presentation as opposed to the adoption of these procedures.

In this regard, a current research project at the University of Utah, to design and build hardware to perform the hidden surface calculations, is very promising. Currently, the hidden surface computations require from one to two minutes of PDP-10 time for each picture. The hardware should accomplish the same task in 1/30 of a second. This will bring computer produced movies into their own, and make possible the recording of computer simulations in real time.

ACKNOWLEDGEMENT

The work presented here is part of a continuing effort at the University of Utah in graphics. This effort, sponsored by the Advanced Research Projects Agency, has produced a software/hardware system which is conducive to application studies. Pictures presented in this paper are a result of the efforts of many people in developing the basic software and hardware systems. In particular, appreciation is expressed to Ronald Resch whose program supplied the geometry of the folded plate system in the flat configuration and called the display routines for those pictures, to Mike Milochik the photographic engineer, and to Martin Yonke and Mike Dervage for assistance in making camera and scope adjustments. The author is also indebted to Dr. David C. Evans, Chairman of Computer Science, for creating the opportunity for this work to be done.

REFERENCES

1. R. D. Resch and H. N. Christiansen, "The Design and Analysis of Kinematic Folded Plate Systems," Proc. Symposium for Folded Plates and Prismatic Structures, International Association for Shell Structures, Vienna, Austria, Oct. 1970.

2. S. Timoshenko and D. H. Young, Theory of Structures, p. 231, McGraw-Hill Book Company, New York, 1945.

3. A. F. Smith, "Method for Computer Visualization," AMC Technical Report No. 8436-TM-2, Electronic Systems Laboratory, M.I.T., September 1960.

4. T. E. Johnson, "Sketchpad III: Three Dimensional Graphical Communication with a Digital Computer," Report ESL-TM-173, Electronic Systems Laboratory, M.I.T., June 1963.

5. L. G. Roberts, "Machine Perception of Three-Dimensional Solids, "Technical Report No. 315 Lincoln Laboratory, M.I.T., 22 May 1963.

6. G. W. Romney, "Computer Assisted Assembly and Rendering of Solids," Dept. Computer Science, Univ. of Utah, Salt Lake City, Tech. Rep. TR 4-20, 1970.

7. J. E. Warnock, "A Hidden Surface Algorithm for Computer Generated Halftone Pictures," Dept. Computer Science, Univ. of Utah, Salt Lake City, Tech. Rep. 4-15 June 1969.

8. G. S. Watkins, "A Real Time Visible Surface Algorithm," Dept. Computer Sci., Univ. of Utah, Salt Lake City, Tech. Rep. UTEC-CSc-70-101, July 1970.

9. R. S. Rougelot and R. Shoemaker, "G.E. Real Time Display," General Electric Co., Syracuse, N. Y., NASA Rep. NAS 9-3916.

10. MAGI, Mathematical Applications Group Inc., "3-D Simulated Graphics," Datamation, Vol. 14, Feb. 1968, p. 69.

11. P. G. Comba, "A Procedure for Detecting Intersections of Three Dimensional Objects," IBM New York Scientific Center, New York, N.Y., Rep. 39.020, Jan. 1967.

12. R. A. Weiss, "Be Vision, A Package of IBM 7090 Fortran Programs to Draw Orthographic Views of Combinations of Planes and Quadric Surfaces," Jour. Ass. Comput. Mach, Vol. 13, April 1966, pp. 194-204.

13. R. Mahl, "Visible Surface Algorithms for Quadric Patches," Dept. Computer Science, Univ. of Utah, Salt Lake City, Tech. Rep. UTEC-CSc-70-111, Dec. 1970.

14. H. Gouraud, "Computer Display of Curved Surfaces," Unpublished Ph.D. Thesis Dept. Computer Science, Univ. of Utah, Salt Lake City, June 1971.

15. R. J. Sanford and A. J. Durelli, "Interpretation of Fringes in Stress-Holo-Interferometry," Experimental Mechanics, Vol. 11, April 1971, pp. 3-8.